Journal of Hydroscience and Hydraulic Engineering
Vol. 11, No. 2, January, 1994, 1-18

EFFICIENT MASS-CONSERVATIVE NUMERICAL SOLUTION FOR THE TWO-DIMENSIONAL UNSATURATED FLOW EQUATION

By

Le Dinh HONG, Juichiro AKIYAMA, and Masaru URA

Department of Civil Engineering, Kyushu Institute of Technology, Kitakyushu, Japan

SYNOPSIS

An efficient and accurate numerical model for solving the two-dimensional Richards' equation in the mixed form is formulated. The model consists of a finite-difference algorithm coupled with a Newton-Raphson linearization algorithm. The numerical scheme is capable of accurately incorporating boundary conditions of all types in a mass-conservative form. Included in the formulation are simple, yet effective algorithms for handling problems associated with the presence of seepage faces and for updating nodal pressure heads during nonlinear iterations. Four test examples are presented to demonstrate the performance of the model. The examples illustrate the improved accuracy of the present solutions compared to the corresponding pressure head-based solutions and the superiority of the present linearization algorithm over existing algorithms for handling nonlinearities of the problems.

INTRODUCTION

Most groundwater is located in the saturated zone, however, it is the unsaturated zone through which water recharges the saturated zone. In typical flow situations, large variations in pressure head and/or soil constitutive relationships render Richards' equation, which governs flows in the unsaturated zone, severely nonlinear. Consequently, any or all of such associated numerical difficulties as iterative convergence problems, numerical oscillations, and large mass balance errors often arise.

Common numerical models to Richards' equation have been developed based on the pressure head-based form and moisture content-based form. Pressure head-based models are applicable to flows in saturated-unsaturated zones and layered zones, but often incur large mass balance errors (Celia et al. (2), Hills et al. (6)). On the other hand, moisture content-based models perfectly conserve mass within the flow domain, but are not applicable to flows in saturated zones, and not directly applicable to flows in layered zones due to discontinuities in moisture content-profiles at the interfaces of layers.

Allen and Murphy (1) pointed out that numerical models based on the mixed form of Richards' equation can guarantee mass balance while having no limitations when applied to field problems. Difficulties which arise in pressure head-based models when attempting to properly evaluate the specific moisture capacity term for conserving mass are naturally circumvented. However, for the finite-element collocation method introduced by Allen and Murphy (1) it is difficult to incorporate the Neumann conditions at boundaries since no boundary integral arises in the formulation. In addition, the slow convergence rate of the Newton-like iteration was also reported. Despite the drawbacks mentioned, Allen and Murphy (1) provided relevant arguments for asserting the advantages of numerical models based on the mixed form of Richards' equation.

The improved numerical behavior of a mixed-based model was later demonstrated in Celia et al. (2). The one-dimensional Richards' equation in the mixed form as

well as in the pressure head-based form was solved using the finite-difference and linear finite-element methods coupled with the modified Picard iteration. The mixed-based solution was shown not only to conserve mass but also to be insensitive to time step size.

In what follows, a numerical model for solving the two-dimensional Richards' equation in the mixed form is formulated. The equation is discretized using the finite-difference method. The Newton-Raphson iteration is adopted to linearize the resulting nonlinear equation. Accurate incorporation of boundary conditions in a mass-conservative form is discussed. An algorithm for handling seepage face problems, where location of the exit point is also part of the solution, is presented. Included in the formulation is a simple, yet effective algorithm for nonlinear updating nodal pressure heads. The efficiency and accuracy of the present model are tested against existing solutions through four examples. The model is developed for unsaturated flows, however, its application to variably saturated flows is straightforward.

GOVERNING EQUATION

The two-dimensional continuity equation for an infinitesimal element of a porous medium, without sources and sinks within the flow domain, can be written as

$$\partial \theta / \partial t + \partial V_k / \partial x_k = 0 \qquad (1)$$

where θ = (volumetric) moisture content; x_k = spatial coordinate ($k = 1, 2$); V_k = Darcy velocity or specific flux; and t = elapsed time. Herein, the repeated index in any product of terms indicates the summation over its possible range of values (i.e. 1 and 2), unless otherwise stated.

Implicit in Eq. (1) are the assumptions: (1) the compressibilities of medium and water are negligible; (2) the porosity and water density are constant; and (3) the air phase is stagnant and at atmospheric pressure.

The Darcy velocity for flows in a homogeneous isotropic medium can be expressed by

$$V_k = - K(\partial \psi / \partial x_k - e_k) \qquad (2)$$

where ψ = pressure head; K = hydraulic conductivity; and e_k = unit vector in the x_2 direction which is oriented positively downwards.

Substituting Eq. (2) into Eq. (1) leads to the Richards' equation in the mixed form;

$$\partial \theta / \partial t - \partial [K(\partial \psi / \partial x_k - e_k)] / \partial x_k = 0 \qquad (3)$$

In Eqs. (2) and (3) K and θ are related to ψ by nonlinear functions (i.e. soil constitute relationships), which depend on the type of soil. The degree of nonlinearity of the problem depends on the extent of variations in values of K and/or θ over the possible range of ψ within the flow domain. For highly nonlinear problems, a small change in pressure head may result in significant variations in values of $K(\psi)$ and/or $\theta(\psi)$.

The initial and boundary conditions may be given by

$$\psi(x_k, t = 0) = \psi_o(x_k) \qquad \text{on } \Omega \qquad (4)$$

$$\psi(x_k, t > 0) = \psi_b(x_k, t) \qquad \text{on } \Gamma_1 \qquad (5)$$

$$V_k n_k = V_n(x_k, t > 0) \qquad \text{on } \Gamma_2 \qquad (6)$$

where Ω = flow domain; $\Gamma = \Gamma_1 \cup \Gamma_2$ = boundary of Ω; ψ_o = initial pressure head prescribed on the flow domain; ψ_b = pressure head prescribed on the Dirichlet boundary segment Γ_1; V_n = prescribed velocity normal to the Neumann boundary segment Γ_2; and n_k = outward unit vector normal to the boundary segment Γ_2. The

sign convention for boundary flux is positive for mass withdrawal from and negative for mass injection into the flow domain.

FINITE-DIFFERENCE FORMULATION

Assume that the flow domain which has one unit width normal to the plane of flows is divided into a number of small rectangular blocks, and nodes are placed at the centers of blocks. Hereafter, the coordinate x_1 is replaced by x, and x_2 by z. The finite-difference approximation to Eq. (1) for a typical block (i,j) indicated in Fig. 1 can be written as

$$(\theta_{i,j}^{n+1}-\theta_{i,j}^{n})/\Delta t + (V_{III}^{*}-V_{I}^{*})/\Delta x + (V_{IV}^{*}-V_{II}^{*})/\Delta z = 0 \quad (7)$$

where n = previous time level; n+1 = current time level; and * = superscript used to denote time averaged values; $\theta_{i,j}$ = moisture content at the block (i,j); V_I^*, V_{II}^*, V_{III}^*, V_{IV}^* = time-averaged velocities normal to the interblocks I, II, III, IV, respectively; x, z = Cartesian coordinates; Δx, Δz = nodal spacings in the x, z directions, respectively; and Δt = time step size.

The time-averaged value for an arbitrary velocity can be determined by

$$V^{*} = \omega V^{n+1} + (1 - \omega)V^{n} \quad (8)$$

where ω = time-weighting factor (ω = 0, 0.5, and 1 correspond to the explicit, Crank-Nicolson, and fully implicit schemes, respectively).

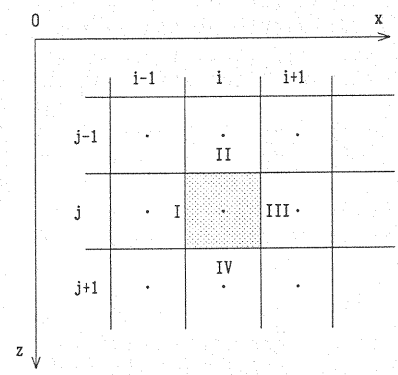

Fig.1 Finite-difference grid

The discretized form of a typical velocity V_{IV} (Fig. 1) at any instant is

$$V_{IV} = - K_{IV} [(\psi_{i,j+1} - \psi_{i,j}) - \Delta z]/\Delta z \quad (9)$$

where K_{IV} = hydraulic conductivity evaluated at the interblock IV between the two blocks (i,j) and (i,j+1). The discretized forms of the velocities V_I, V_{II}, and V_{III} can be derived in a similar way.

With the discretization procedure just described, Eq. (7) can be rewritten as

$$\begin{aligned}
&\omega \Delta t/\Delta x^2[- K_{III}^{n+1}(\psi_{i+1,j}^{n+1} - \psi_{i,j}^{n+1}) \\
&\qquad + K_I^{n+1}(\psi_{i,j}^{n+1} - \psi_{i-1,j}^{n+1})] \\
&+ \omega \Delta t/\Delta z^2[- K_{IV}^{n+1}(\psi_{i,j+1}^{n+1} - \psi_{i,j}^{n+1} - \Delta z) \\
&\qquad + K_{II}^{n+1}(\psi_{i,j}^{n+1} - \psi_{i,j-1}^{n+1} - \Delta z)] \\
&+ \theta_{i,j}^{n+1} - \theta_{i,j}^{n} + (1 - \omega)\Delta t/\Delta x [V_{III}^{n} - V_{I}^{n}] \\
&\qquad + (1 - \omega)\Delta t/\Delta z [V_{IV}^{n} - V_{II}^{n}] = 0 \quad (10)
\end{aligned}$$

There exist various weighting means of estimating the interblock hydraulic conductivity K_{IV} (see e.g. Cooley (3), Haverkamp and Vauclin (4), Narasimhan and Witherspoon (12)). Among them the geometric mean, i.e.

$$K_{IV} = [K(\psi_{i,j})K(\psi_{i,j+1})]^{1/2} \quad (11)$$

is the best estimate for K_{IV} because of little weighting errors incurred as nodal spacing changes (Haverkamp and Vauclin (4)). However, owing to the occurrence of the product $K(\psi_{i,j})K(\psi_{i,j+1})$, the mean of the two hydraulic conductivities tends

to be strongly weighted toward the lower one. For many problems of infiltration into initially dry soils the water can not drain downward. This results in a non-physical buildup of water pressure at the ground surface. Consequently, the iteration fails to converge to a solution. In this study, the interblock hydraulic conductivity is estimated by the arithmetic mean;

$$K_{I\nu} = 0.5[K(\psi_{i,j}) + K(\psi_{i,j+1})] \qquad (12)$$

This results in a numerical model which is applicable to all flow problems.

Since θ^{n+1} and K^{n+1} are nonlinear functions of ψ^{n+1}, a proper linearization with or without iteration must be introduced into Eq. (10). The Newton-Raphson iteration is often recommended for highly nonlinear problems, for which the Picard iteration may fail to converge or provide low convergence rates (Huyakorn et al. (9), Kaluarachchi and Parker (10), Paniconi et al. (13)). Furthermore, Paniconi et al. (13) found that the Newton-Raphson iteration is more robust and less sensitive to nonlinearities and initial solution estimates than the Picard iteration. The advantages of the Newton-Raphson iteration lie in the enhanced convergence rate and the simplicity of the algorithm for updating nodal pressure heads.

Let the left-hand side of Eq. (10) denote a function $R_{i,j}^{n+1}$. Application of the Newton-Raphson iteration involves expanding Eq. (10) about the rth iteration solution $\psi^{n+1,r}$ in a Taylor series which is truncated after first derivatives. This procedure results in

$$R_{i,j}^{n+1,r} + (\partial R_{i,j}^{n+1,r}/\partial \psi_m)\delta\psi_m = 0 \qquad (13)$$

where r = previous iteration level; r+1 = current iteration level; $\psi^{n+1,r}$ = pressure head after the rth iteration; and $\delta\psi = \psi^{n+1,r+1} - \psi^{n+1,r}$ = iterative increment, i.e. change in pressure head between two iterations. In Eq. (13) the index m indicates the summation over five nodes: (i,j), (i-1,j), (i+1,j), (i,j-1), and (i,j+1). The term $R_{i,j}^{n+1,r}$ is often referred to as the residual since it measures the amount by which the solution at the rth iteration fails to satisfy the nonlinear equation (Eq. 10).

The linearization procedure just described enables us to recast Eq. (10) into a simple form as

$$E_{i,j}^{n+1,r}\delta\psi_{i-1,j} + F_{i,j}^{n+1,r}\delta\psi_{i+1,j} + G_{i,j}^{n+1,r}\delta\psi_{i,j-1} + H_{i,j}^{n+1,r}\delta\psi_{i,j+1} + I_{i,j}^{n+1,r}\delta\psi_{i,j} + R_{i,j}^{n+1,r} = 0 \qquad (14)$$

where

$$E_{i,j}^{n+1,r} = \omega\Delta t/\Delta x^2[-K_I^{n+1,r} + D_{i-1,j}^{n+1,r}(\psi_{i,j}^{n+1,r} - \psi_{i-1,j}^{n+1,r})/2] \qquad (15a)$$

$$F_{i,j}^{n+1,r} = \omega\Delta t/\Delta x^2[-K_{III}^{n+1,r} - D_{i+1,j}^{n+1,r}(\psi_{i+1,j}^{n+1,r} - \psi_{i,j}^{n+1,r})/2] \qquad (15b)$$

$$G_{i,j}^{n+1,r} = \omega\Delta t/\Delta z^2[-K_{II}^{n+1,r} + D_{i,j-1}^{n+1,r}(\psi_{i,j}^{n+1,r} - \psi_{i,j-1}^{n+1,r} - \Delta z)/2] \qquad (15c)$$

$$H_{i,j}^{n+1,r} = \omega\Delta t/\Delta z^2[-K_{I\nu}^{n+1,r} - D_{i,j+1}^{n+1,r}(\psi_{i,j+1}^{n+1,r} - \psi_{i,j}^{n+1,r} - \Delta z)/2] \qquad (15d)$$

$$I_{i,j}^{n+1,r} = C_{i,j}^{n+1,r} + \omega\Delta t/\Delta x^2[K_I^{n+1,r} + D_{i,j}^{n+1,r}(\psi_{i,j}^{n+1,r} - \psi_{i-1,j}^{n+1,r})/2]$$

$$+ \omega \Delta t/\Delta x^2[K_{III}^{n+1,r} - D_{i,j}^{n+1,r}(\psi_{i+1,j}^{n+1,r} - \psi_{i,j}^{n+1,r})/2]$$

$$+ \omega \Delta t/\Delta z^2[K_{II}^{n+1,r} + D_{i,j}^{n+1,r}(\psi_{i,j}^{n+1,r} - \psi_{i,j-1}^{n+1,r} - \Delta z)/2]$$

$$+ \omega \Delta t/\Delta z^2[K_{IV}^{n+1,r} - D_{i,j}^{n+1,r}(\psi_{i,j+1}^{n+1,r} - \psi_{i,j}^{n+1,r} - \Delta z)/2] \quad (15e)$$

$$R_{i,j}^{n+1,r} = \theta_{i,j}^{n+1,r} - \theta_{i,j}^{n}$$

$$+ \omega \Delta t/\Delta x(V_{III}^{n+1,r} - V_{I}^{n+1,r}) + (1 - \omega)\Delta t/\Delta x(V_{III}^{n} - V_{I}^{n})$$

$$+ \omega \Delta t/\Delta z(V_{IV}^{n+1,r} - V_{II}^{n+1,r}) + (1 - \omega)\Delta t/\Delta z(V_{IV}^{n} - V_{II}^{n}) \quad (15f)$$

where $C = d\theta/d\psi$ = specific moisture capacity; and $D = dK/d\psi$ = tangent slope of the K-ψ curve. The specific moisture capacity C in Eq. (15e) is computed analytically from the soil constitutive function $\theta(\psi)$, which is consistent with the Taylor series expansion (Eq. 13). If all terms containing the coefficients $D_{i,j}$ in Eqs. (15a-e) are neglected, the iteration is referred to as the Newton-like iteration by Allen and Murphy (1) or the modified Picard iteration by Celia et al. (2). Such an iteration provides a linearization of first-order accuracy.

Writing Eq. (14) for all (i,j) leads to a system of linearized equations as

$$A^{n+1,r}\delta\psi = -R^{n+1,r} \quad (16)$$

where $A^{n+1,r}$ = matrix of coefficients; $\delta\psi$ = unknown vector; and $R^{n+1,r}$ = residual vector. The matrix equation (Eq. 16) is solved using a direct solver decomposition taking into account the banded feature of the matrix $A^{n+1,r}$.

For convergence in iteration, it is required that

$$|R_{i,j}^{n+1,r}| < \varepsilon \qquad \text{for all (i,j)} \quad (17)$$

where ε = water content convergence tolerance. Because a sufficiently small value of ε (say, 10^{-5}) is usually imposed, Eq. (17) (also refer to Eq. 15f) practically represents the principle of mass conservation for an arbitrary block (i,j). The mixed-based solution, therefore, conserves mass balance regardless of time step size and nodal spacings. These advantages are very significant for field-scale simulations, where the use of large nodal spacings is often required because of limitations in computer storage capacity, and the use of large time step size can greatly reduce computer time.

SOLUTION STRATEGY

Boundary Treatment

a. Flux-Type Boundary Condition

In the proposed scheme, the grid is arranged in such a manner that boundaries of the flow domain fall on interblocks. Therefore, flux (or velocity)-type boundary conditions can be naturally incorporated into Eq. (7).

b. Pressure Head-Type Boundary Condition

Without loss of generality, one can consider a one-dimensional problem in the x direction. Assume that ψ_b is the pressure head prescribed at x = 0 (Fig. 2). With the aid of the quadratic interpolation using pressure heads at x = 0, $\Delta x/2$, and $3\Delta x/2$, the pressure-head gradient at x = 0 is determined by

$$\partial\psi/\partial x|_{x=0} = (-8\psi_b/3 + 3\psi_1 - \psi_2/3)/\Delta x \quad (18)$$

From Eq. (2), one obtains the velocity (or flux) at x = 0 as

$$V_x \mid_{x=0} = - K(\psi_b)[(- 8\psi_b/3 + 3\psi_1 - \psi_2/3)/\Delta x - e_1] \qquad (19)$$

The advantages of the treatment described above are:

(a) Assume that at some boundary segment the pressure head prescribed is constant with time. However, the moisture contents at blocks adjacent to that boundary segment are not necessarily constant. Eq. (19) enables us to account for the variation with time of the moisture contents at the boundary blocks in the approximation. In contrast, for other alternatives where nodes fall on boundaries, the moisture contents at the boundary blocks always assume constant values.

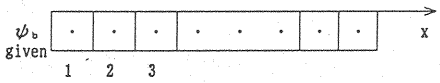

Fig. 2 Definition sketch used for treatment of pressure head-type boundary condition

(b) For flow situations where seepage faces are present, Dirichlet and Neumann conditions along the potential seepage faces can be easily implemented.

Treatment of Seepage Face

Under transient conditions, the length of the seepage face varies with time in such a manner that the location of the exit point E (Fig. 3) is not known a priori but must be computed as part of the solution. Along any portion of the potential seepage face, two conditions must be simultaneously satisfied as

(a) If a zero-normal flux (V_{sf} = 0) is imposed at the boundary, the computed pressure head ψ_{sf} at that boundary must be negative. For short, we term this boundary as type-1 boundary.

(b) If a zero-pressure head (ψ_{sf} = 0) is imposed at the boundary, the computed normal flux V_{sf} at that boundary must be positive. This boundary is termed as type-2 boundary.

Without loss of generality, assume that the potential seepage face is located at the right face of the flow domain (Fig. 3). For the present purpose, the location of the boundary segment in the z direction is immaterial. Therefore, the index used to denote the location of the row being considered is dropped. To incorporate the boundary conditions described above the following iteration algorithm is proposed:

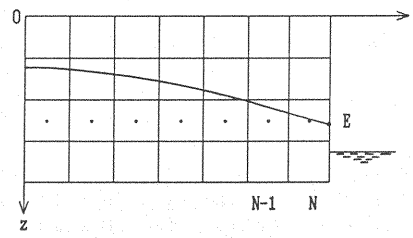

Fig. 3 Definition sketch used for treatment of seepage face

(a) At the beginning of each time step, the boundary-condition type for each boundary block is assumed to be identical to that obtained at the end of the previous time level.

(b) At the end of each iteration, the following conditions will be checked for every boundary block:

- For type-1 boundary, if $\psi_{sf} = (9\psi_N - \psi_{N-1})/8$ is positive, the boundary-condition type is switched to type-2, where N = number of blocks in the row being considered.
- For type-2 boundary, if $V_{sf} = - K_s(- 3\psi_N + \psi_{N-1}/3)/\Delta x$ is negative, the boundary-condition type is switched to type-1, where K_s = saturated hydraulic conductivity.

The expressions for ψ_{sf} and V_{sf} have been derived with the aid of quadratic interpolations. If none of the boundary-condition types needs to be altered and the convergence condition for the whole flow domain (to be detailed below) is satisfied at certain iteration, the iteration is then terminated. Otherwise, new iteration is required.

The (free) water surface, where the pressure head equals zero, has no direct relation with the calculation algorithm. For graphically illustrating purposes,

the position of the water surface is determined by simple linear interpolations from the nodal pressure heads having opposite signs at two successive blocks in the vertical direction (Fig. 3). The height of the seepage face, i.e. the position of the exit point E, is computed by a quadratic extrapolation from the heights of the water surface at the first three interior columns from the potential seepage face.

Updating Nodal Pressure Heads

To advance the approximate solution from the time level n to the next level (n+1) the following algorithm is proposed:

Step 1: At the beginning of each time step (r = 0), replace (n+1) by n. Estimate the initial nodal pressure heads by

$$\psi_{i,j}^{n+1,0} = \psi_{i,j}^{n} + \eta(\psi_{i,j}^{n} - \psi_{i,j}^{n-1}) \qquad (20)$$

where η = empirical function.

Step 2: Compute the residual vector $R^{n+1,r}$.

Step 3: If $|R_{i,j}^{n+1,r}| < \varepsilon$ for all (i,j), accept $\psi_{i,j}^{n+1,r}$ as the converged value, then go to step 1. Otherwise, go to step 4.

Step 4: Compute the matrix of coefficients $A^{n+1,r}$, then solve Eq. (16) for $\delta\psi$.

Step 5: Update the nodal pressure heads by

$$\psi_{i,j}^{n+1,r+1} = \psi_{i,j}^{n+1,r} + \delta\psi_{i,j} \qquad (21)$$

Then go to step 2.

The algorithm for nonlinear updating nodal pressure heads (Eq. 21) is very simple, yet effective, because it results from the second-order accurate linearization (Eq. 13).

If the iterative increment $\delta\psi_{i,j}$ is used for the convergence check, step 3 is omitted. Instead, another step (step 4a) is inserted between step 4 and step 5 as follows:

Step 4a: If $|\delta\psi_{i,j}| < \varepsilon_p$ for all (i,j), accept $\psi_{i,j}^{n+1,r}$ as the converged value, then go to step 1. Otherwise, go to step 5. ε_p is the pressure head convergence tolerance.

Either ε and/or ε_p can be used as a convergence criterion. The use of ε is preferred because ε provides information, prior to obtaining the solution, about the mass balance error in the numerical results regardless of time step size and nodal spacings to be used in the simulation.

At the beginning of each time step, the initial pressure head for each node in the flow domain is estimated by a linear extrapolation from the two most recent calculated values (Eq. 20), in which the function η is empirically defined by

$$\eta = \chi[1 + \ln(\Delta t_{n+1}/\Delta t_n)] \qquad (22)$$

where Δt_n = previous time step size; Δt_{n+1} = current time step size; χ = 0.6 = an empirical coefficient; and ln = natural logarithm.

The role that the coefficient χ plays in the convergence rate is next clarified. Without loss of generality, assume that Δt is constant. At the start of each time step, if we simply assign ψ^n to $\psi^{n+1,0}$ by setting χ = 0 in Eq. (22), Eq. (15f) becomes

$$R_{i,j}^{n+1,0} = \Delta t[(V_{III}^{n} - V_{I}^{n})/\Delta x + (V_{IV}^{n} - V_{II}^{n})/\Delta z] \qquad (23)$$

which, in general, differs from zero. Therefore, the above estimation is not preferable. We also do not expect that the change in pressure head at each node between two time levels is always of the same magnitude during simulation, i.e. χ = 1. These reasons suggest the "optimal" value of χ to be roughly 0.6. Eq. (22) with χ = 0.6 greatly enhances the convergence rate during iteration as shown in an earlier study (Hong et al. (7)).

Time-Stepping Scheme

For highly nonlinear problems, the pressure head in the flow domain varies rapidly in the early stages of the solution process, that often results in convergence problems. To circumvent this, it is desirable to use small time step sizes during early time of simulations, thereafter time step sizes are gradually increased. Herein we employ the following time stepping scheme: the computation is started with an initial time step size Δt_0, which is arbitrarily chosen provided the convergence can be achieved. For subsequent time steps, time step sizes are increased in the following manner:

$$\Delta t_{n+1} = \Delta t_n \qquad \text{if } I_n \geqq I_{max} \tag{24a}$$

$$\Delta t_{n+1} = \zeta \Delta t_n \qquad \text{if } I_n < I_{max} \tag{24b}$$

where I_n = number of iterations required for the previous time step. In our computations, ζ = 1.2 and I_{max} = 8 are imposed. The value of ζ usually ranges from 1.04 to 1.4, and the value of I_{max} from 5 to 12 (Huyakorn et al. (8), Kaluarachchi and Parker (10)). The time step sizes are also set smaller than a prescribed maximum value Δt_{max}. The determination of the value of Δt_{max} depends on the intermediate information needed from the solution. In addition, Δt_{max} should not be too large to degrade the accuracy of the solution.

Mass-Balance Check

Various errors may occur in the course of obtaining a numerical solution. Possible sources of errors are: (1) discretization errors; (2) inaccuracy in incorporating boundary conditions, including failure to reproduce the geometric irregularities of the flow domain; (3) imposing relatively large value of the convergence tolerance; and (4) programming errors. Thus, it is necessary to have a means of verifying the results. The mass balance check provides an independent means to assess accuracy of the numerical solution and should be part of every program. However, it should be noted that the mass balance check provides a necessary but not sufficient condition for certifying the accuracy of the solution. The (relative) mass balance error is defined by the ratio $|W_\Omega - W_\Gamma| / W_\Omega$, where W_Γ = net cumulative flux into the flow domain through its boundary; and W_Ω = change in amount of water within the flow domain.

ILLUSTRATIVE EXAMPLES

Four examples will be presented to examine relative performance of the present model and existing models. The computational parameters (time step size, nodal spacings, convergence tolerance, and time-weighting factor) were the same as those used by the referred authors, unless otherwise stated. For comparison purposes, both the Newton-Raphson and modified Picard iterations were used in the computations. The number of time steps for each simulation and the average number of iterations per each time step are presented in Table 1.

Table 1 Number of time steps and number of iterations per time step for the Newton-Raphson and modified Picard iterations

	Total simulation time	Newton-Raphson iteration		Modified Picard iteration	
		Number of time steps	Iterations per time step	Number of time steps	Iterations per time step
Ex. 1	0.8 hrs	55	2.82	93	7.17
Ex. 2	3.05 days	31	6.8	31	54.
Ex. 3	2. hrs	37	1.62	37	1.62
Ex. 4	8. hrs	133	2.53	142	5.30

Example 1: One- and Quasi-Two-Dimensional Infiltration

This problem concerns a one-dimensional infiltration into a uniform sand column, for which the quasi-analytical solution by Philip (14) as well as the one-step ψ-based numerical solution by Haverkamp et al. (5) are available. This example was selected to verify the accuracy of the proposed scheme. The computational parameters are given in Table 2. Time step sizes were generated by the time-stepping scheme. Note that we implemented the free-drainage condition at the lower boundary, which could be more adequate than the condition $\psi = \psi_0$, as also asserted by McCord (11).

Calculated moisture content profiles at times t = 0.1, 0.2, and 0.8 hr are presented in Fig. 4. Also included in Fig. 4 are the moisture content profiles obtained by Philip and by Haverkamp et al. (both were taken from Table 3 in Haverkamp et al. (5)). The agreement among the three results is excellent. It may be noted that the time step sizes in our computation were increased gradually from 10 sec to 60 sec, while a much smaller time step size of 5 sec was used in Haverkamp et al.'s computation (5).

To further test the performance of the proposed model, we again solved the flow problem in the two-dimensional domain (20 cm, 100 cm). The initial and boundary conditions were uniformly distributed in the x direction. The zero-flux conditions were imposed along the two vertical boundaries of the flow domain. The computational parameters were those used for the one-dimensional computation except that the nodal spacings were $\Delta x = \Delta z = 2$ cm. Since all calculated results are uniformly distributed in the x direction, the moisture content profiles in the x direction will not be shown.

Table 2 Computational parameters used in the Example 1

$$K = K_s \frac{A}{A + |\psi|^m}$$

$$\theta = \theta_r + \frac{B(\theta_s - \theta_r)}{B + |\psi|^n}$$

K_s = 34 cm/hr
$A = 1.175 \times 10^6$, $m = 4.74$
$\theta_s = 0.287$, $\theta_r = 0.075$
$B = 1.611 \times 10^6$, $n = 3.96$
$\theta(z, t = 0) = 0.1$
$\psi(0\ \text{cm}, t > 0) = -20.73$ cm
$\partial\psi(100\ \text{cm}, t > 0)/\partial z = 0$
Length of column = 100 cm
$\Delta z = 1$ cm
$\Delta t_0 = 10$ s, $\Delta t_{max} = 60$ s
Tolerance $\varepsilon = 1.\times 10^{-5}$
Time-weighting factor $\omega = 1$

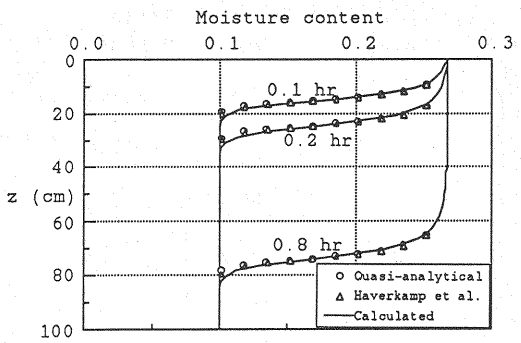

Fig. 4 Comparison of moisture content profiles

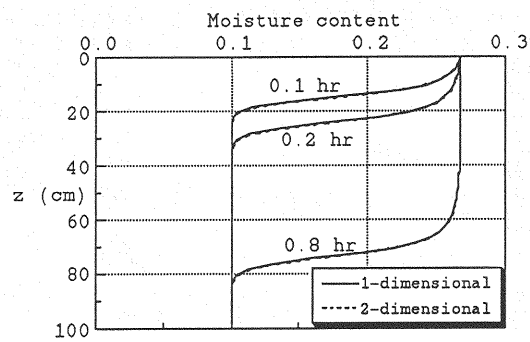

Fig. 5 Computed moisture content profiles by the one and two-dimensional simulations

Fig. 5 presents the moisture content profiles at times t = 0.1, 0.2, and 0.8 hr obtained by our one- and two-dimensional computations. The two results are virtually indistinguishable even though a coarse grid was employed in the two-dimensional computation. It appears that the mixed-based model conserves mass within the flow domain, which, in turn, could substantially reduces the spatial-discretization errors associated with large nodal spacings. The infiltration rate and cumulative infiltration per unit area obtained by our one- and two-dimensional computations and by Haverkamp et al. (5) are presented in Figs. 6a and 6b, respectively. The agreement is again excellent. Philip's solution was not included

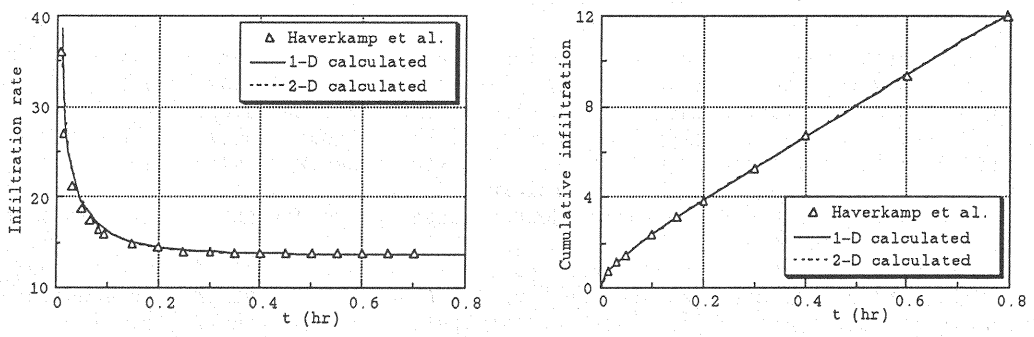

(a) (b)

Fig. 6 Comparison of (a) infiltration rate ($cm^3/hr/cm^2$) and (b) cumulative infiltration (cm^3/cm^2)

because it diverges at time $t \geqq 0.3$ hr (for further information see Haverkamp et al. (5)). The mass balance errors in our solutions are less than 2×10^{-5}.

Example 2: Quasi-Two-Dimensional Infiltration

This problem was previously examined by Cooley (3), who employed a subdomain finite-element method to solve the ψ-based Richards' equation. Nonlinear soil properties were treated by a Newton-like iteration. To avoid convergence problems due to severe oscillations in iterative increments of pressure heads Cooley (3) proposed an empirical nonlinear updating relaxation algorithm which accounts for the maximum convergence error for the entire computational grid. This algorithm was later adopted by Huyakorn et al. (8), Kaluarachchi and Parker (10).

The flow problem is in fact a one-dimensional case, however, 2 blocks in the x direction were used in our computation, which is consistent with Cooley's computation (3). The zero-flux conditions were imposed along the two vertical boundaries of the flow domain. The computational parameters are given in Table 3.

Fig. 7 presents the profiles of water saturation (i.e., moisture content normalized by the saturated moisture content) obtained by our computation and by Cooley (3). The profile at time t = 1.2 hr obtained by Cooley (3) lags slightly behind the present profile, but the deviation is quite considerable at time t = 3.05 hr. As time proceeds the profiles obtained by Cooley (3) exhibit an increasing cumulative-mass loss,

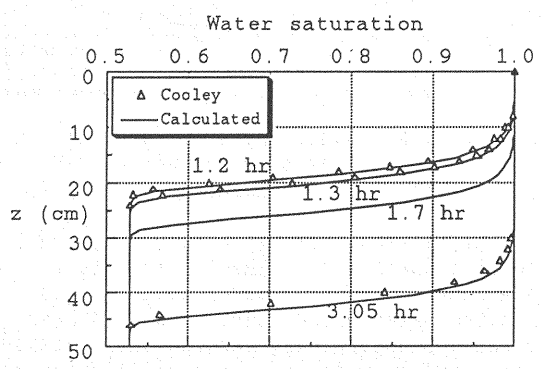

Fig. 7 Comparison of water saturation profiles

Table 3 Computational parameters used in the Example 2

$K = K_s(A/\lvert\psi\rvert)^m$	$\psi \leqq -5.4$ cm
$\theta = \theta_s(A/\lvert\psi\rvert)^n$	$\psi \leqq -5.4$ cm
$K = K_s = 3.125$ cm/hr	$\psi \geqq -5.4$ cm
$\theta = \theta_s = 0.52$	$\psi \geqq -5.4$ cm

A = 5.4, m = 2.6, n = 0.2
$\psi(z, t = 0) = -130.54$ cm
$\psi(0 \text{ cm}, t > 0) = -5.4$ cm
$\partial\psi(49 \text{ cm}, t > 0)/\partial z = 0$
Length of column = 49 cm
$\Delta z = \Delta x = 1$ cm
$\Delta t = 0.1$ hr = constant
Tolerance $\varepsilon_p = 0.001$ cm
Time-weighting factor $\omega = 1$

probably due to large mass balance errors associated with pressure head-based models.

It may be noted that once the front has been established, thereafter it has moved with a theoretical velocity corresponding to a hydraulic gradient of unity. The theoretical front velocity is $v_f = K_s/(\theta_s - \theta_o)$ = 12.755 cm/hr, where K_s = saturated hydraulic conductivity; θ_s = saturated moisture content; and θ_o = initial moisture content. If we adopt Cooley's assumption (3) that the front has been established at time t = 1.2 hr, the front velocity given by Cooley (3) is 12.432 cm/hr, which is 2.53 % lower than v_f. The front velocity obtained by our computation is 23.71/(3.05 - 1.2) = 12.816 cm/hr, which is 0.48 % higher than v_f.

For reference purposes, the infiltration rate and cumulative infiltration per unit area obtained by our computation are presented in Fig. 8 and Table 4. From

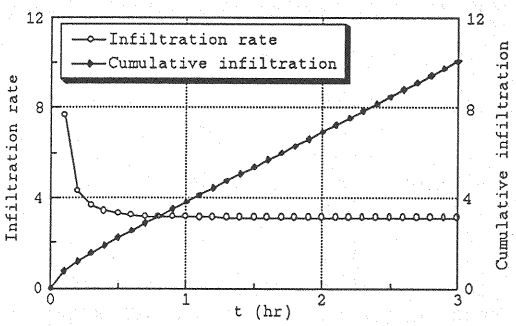

Fig. 8 Computed infiltration rate ($cm^3/hr/cm^2$) and cumulative infiltration (cm^3/cm^2)

Table 4 Computed infiltration rate (I) and cumulative infiltration (V)

Time (hr)	I (cm/hr)	V (cm)	Time (hr)	I (cm/hr)	V (cm)
0	0.	0.	1.6	3.126	5.694
0.1	7.687	0.769	1.7	3.125	6.006
0.2	4.276	1.196	1.8	3.125	6.319
0.3	3.659	1.562	1.9	3.125	6.631
0.4	3.412	1.903	2.0	3.125	6.944
0.5	3.289	2.232	2.1	3.125	7.256
0.6	3.221	2.554	2.2	3.125	7.569
0.7	3.182	2.872	2.3	3.125	7.881
0.8	3.159	3.188	2.4	3.125	8.194
0.9	3.146	3.503	2.5	3.125	8.506
1.0	3.138	3.817	2.6	3.125	8.819
1.1	3.133	4.130	2.7	3.125	9.131
1.2	3.13	4.443	2.8	3.125	9.444
1.3	3.128	4.756	2.9	3.125	9.756
1.4	3.127	5.068	3.0	3.125	10.069
1.5	3.126	5.381	3.05	3.125	10.225

Table 4, we notice that the shape of the front has actually been established at time t = 1.7 hr. Therefore, the front velocity by our computation turns to be 17.31/(3.05 - 1.7) = 12.822 cm/hr, which is 0.52 % higher than v_f. Owing to the discretization errors inherent in the numerical solution, we were not able to obtain the exact front velocity. This comparison, however, demonstrates that the proposed model yields a solution which is more accurate than the ψ-based solution by Cooley (3). The mass balance error in our solution is less than 3×10^{-6}.

It may be noted our model required an average of 6.8 iterations for each time step, while Cooley's model (3) required at least 53 iterations for each time step.

Example 3: Two-Dimensional Drainage from a Square Block

This problem was previously analyzed by Rubin (15), who used an Alternating Direction Implicit (ADI) finite-difference method to solve the ψ-based Richards' equation. The example was selected to demonstrate the performance of the proposed model for a transient flow situation involving a significant variation in the water table position.

Geometry of the flow domain (30 cm, 30 cm), initial and boundary conditions are depicted in Fig. 9. The domain was initially in a static equilibrium. The water level at the right face of the domain was then lowered suddenly, from 30 cm to 10 cm, and maintained at 10 cm thereafter. The computational parameters are given in Table 5. Time step sizes were generated by the time-stepping scheme. Computational parameters were not reported

Table 5 Computational parameters used in the Example 3

$$K = K_s \frac{A}{A + |\psi|^m}$$

$$\theta = 0.6009 - 0.05708 \ln(10.0 - \psi) + 0.0594/\cosh(0.747 + 0.0415\psi) - 0.0132 \exp(0.4055 - 0.20\psi)$$

$K_s = 1.1575\times10^{-5}$ cm/s, A = 400.
m = 2, $\Delta z = \Delta x$ = 2 cm
Δt_o = 10 s, Δt_{max} = 360 s
Tolerance $\varepsilon = 1.\times10^{-5}$
Time-weighting factor ω = 1

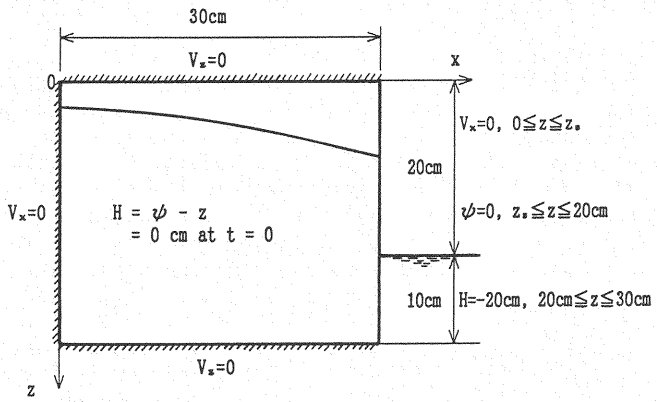

Fig. 9 Problem definition for Example 3

in Rubin (15).

Figs. 10a and 10b present the water table position at t = 2 hr and the time-dependent water table crest (at x = 0), respectively, obtained by our computation and by Rubin (15). The agreement between the two solutions is excellent. The distribution of outflux from the seepage face at t = 2 hr obtained by the two numerical models is presented in Fig. 11. The two results are again in good agreement. It may be noticed that the proposed model is of second-order accuracy in space, the computed flux (or Darcy velocity), therefore, varies linearly between centers of boundaries of blocks. From this observation, the outflux at the water table (z = 20 cm) was computed via a linear extrapolation from the values of

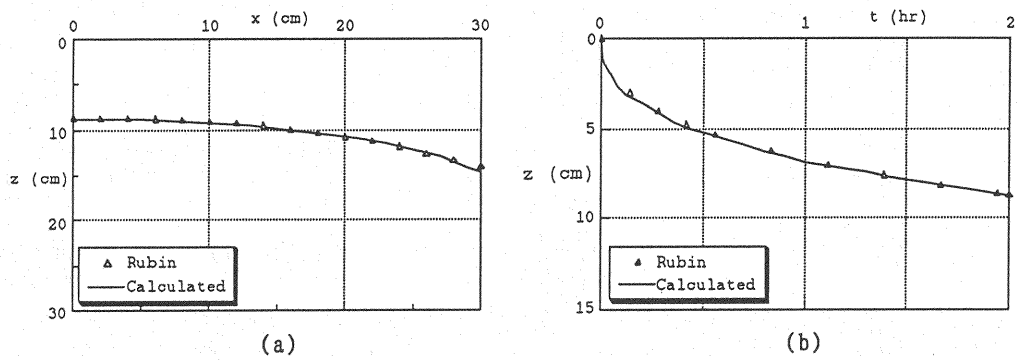

Fig. 10 Comparison of (a) water table position at t = 2 hr and (b) time-dependent water table crest (x = 0)

the outflux at the two blocks adjacent to the water table. For completeness, the computed time-dependent outflow rate and cumulative outflow are plotted in Fig. 12, and the distribution of the hydraulic head within the flow domain at time t = 2 hr is shown in Fig. 13. The mass balance error in our solution is less than 0.2×10^{-5}.

It may be noted from Table 1 that the Newton-Raphson iteration and the modified Picard iteration required identical the number of time steps and number of iterations per time step. This fact could be explained as follows: the Newton-Raphson iteration is mainly implemented to cope with the high nonlinearities of soil properties; the more nonlinear the soil properties are, the more efficient the Newton-Raphson iteration is. In this simulation, the flow domain was fully

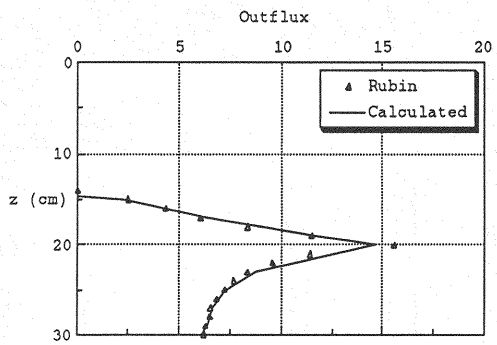

Fig. 11 Comparison of distribution of outflux at t = 2 hr

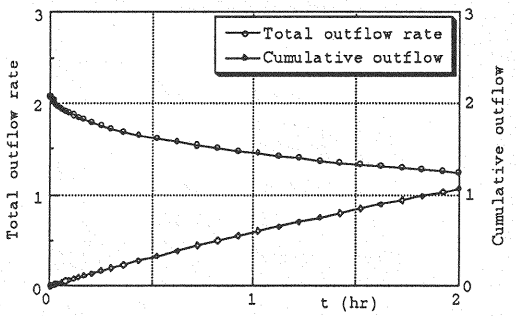

Fig. 12 Computed total outflow rate and cumulative outflow

saturated at t = 0, while the minimum value of pressure head at the end of the simulation was approximately - 8.5 cm (it can be observed from Fig. 13). For such a very mildly nonlinear problem, it is not expected that the Newton-Raphson iteration is computationally more efficient than the modified Picard iteration. This example demonstrates that the proposed model performed well for the situation where the flows simultaneously occur in the unsaturated and saturated zones involving a drastic change in the water table position.

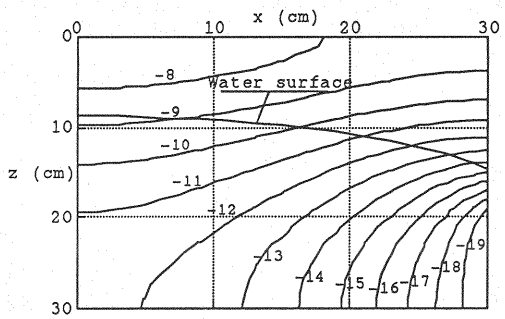

Fig. 13 Computed distribution of hydraulic head at t = 2 hr

Example 4: Two-Dimensional Water Table Recharge

This problem was taken from an experimental and numerical study by Vauclin et al. (16), in which the ψ-based Richards' equation was solved using an ADI finite-difference method. It may be noticed that the pressure head ψ and moisture content θ at the ground surface which were obtained experimentally do not satisfy the soil constitutive relationship $\theta(\psi)$ proposed by Vauclin et al. (16). Due to such an inconsistency, no quantitative comparison will be made in this study. The problem was selected to examine the response of a water table to infiltration from the soil surface.

Geometry of the flow domain (200 cm, 300 cm), initial and boundary conditions are depicted in Fig. 14. The soil slab was initially in a static equilibrium. A constant flux of q_o = 14.8 cm³/hr/cm² was then applied over a width of 50 cm at the ground surface. At the right face of the flow domain, the water level in the ditch was kept at a constant depth of 65 cm. The computational parameters are given in Table 6. Time step sizes were generated by the time-stepping scheme with Δt_o = 10 sec and Δt_{max} = 240 sec. It may be noted that the ADI schemes are unconditionally stable for linear problems, but this is not the case for nonlinear problems. As such, a very small time step size of 10 sec was used by Vauclin et al. (16).

Table 6 Computational parameters used in the Example 4

$$K = K_s \frac{A}{A + |\psi|^m}$$

$$\theta = \theta_s \frac{B}{B + |\psi|^n}$$

K_s = 35 cm/hr
A = 2.99x10⁶, m = 5.
θ_s = 0.3
B = 4.x10⁴, n = 2.9
$\Delta z = \Delta x$ = 10 cm
Δt_o = 10 s, Δt_{max} = 240 s
Tolerance ε_p = 0.01 cm
Time-weighting factor ω = 1

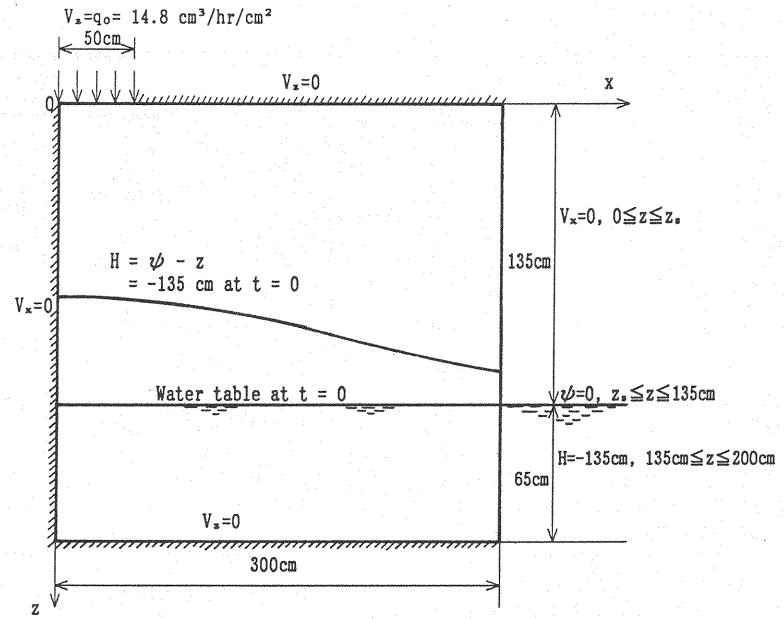

Fig. 14 Problem definition for Example 4

Figure 15 shows the water table position at times t = 2, 3, 4, and 8 hr obtained by our computation and by Vauclin et al. (16). The agreement between the two solutions is satisfactory. The cumulative volumes of water leaving and stored within the soil slab of 5 cm thickness obtained by the two numerical models are presented in Fig. 16. The two results are quite different. It seems difficult to assess the accuracy of the two solutions. However, direct measuring data presented in Fig. 9 in Vauclin et al. (16) shows that the cumulative volumes of water leaving and stored within the soil slab of 5 cm thickness at time t = 8 hr are 15.18 liter and 15 liter, respectively. Thus, the total cumulative influx computed by Vauclin et al. (16) is 30.18 liter, which is nearly 2 % different from the exact value 14.8 cm³/hr/cm² x 50 cm x 5 cm x 8 hr = 29.6 liter. The mass balance error in Vauclin et al.'s solution (16) could be attributed to the poor approximation of the specific moisture capacity C (e.g. Allen and Murphy (1), Celia et al. (2)) and to the ADI procedure as well. Such a solution associated with a large

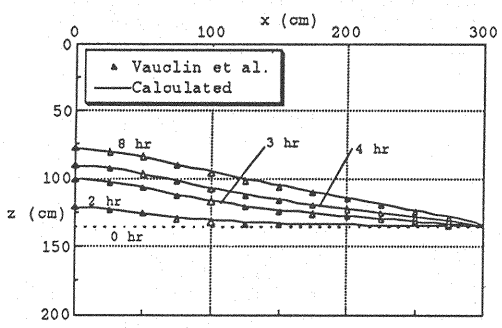

Fig. 15 Comparison of water table position

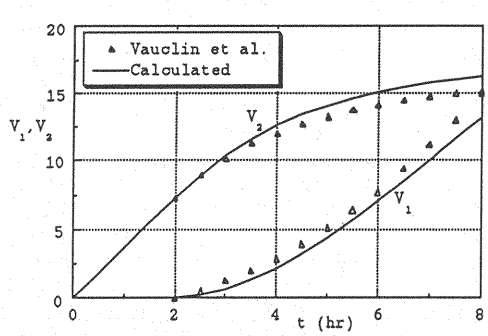

Fig. 16 Comparison of cumulative volumes (liter) of water leaving (V_1) and stored (V_2) within the domain

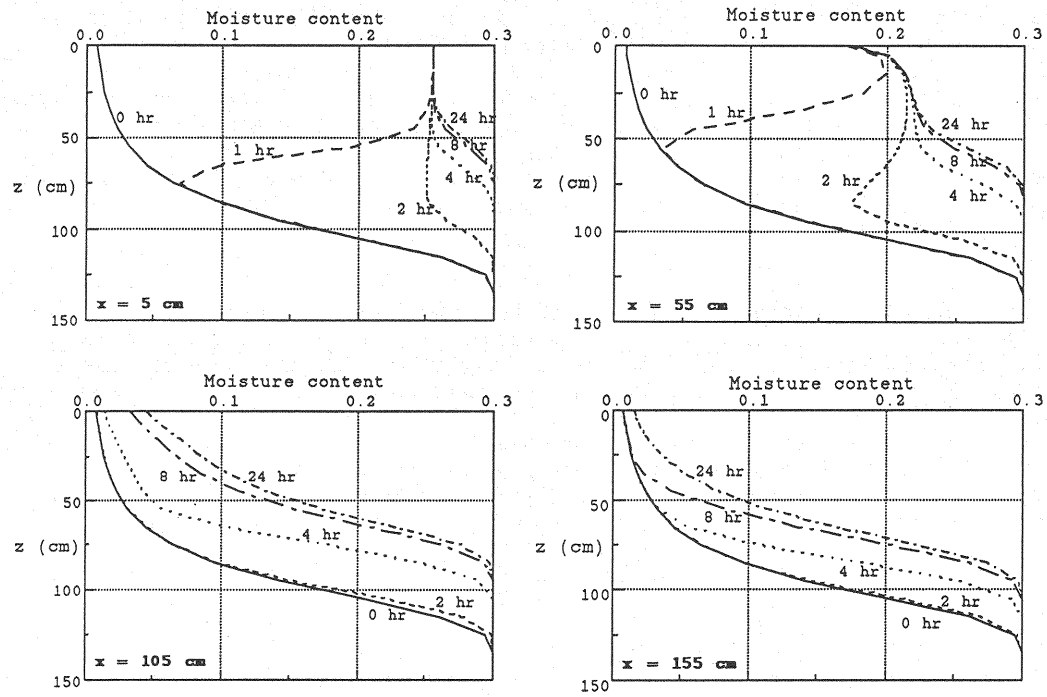

Fig. 17 Computed moisture content profiles
at x = 5, 55, 105, and 155 cm

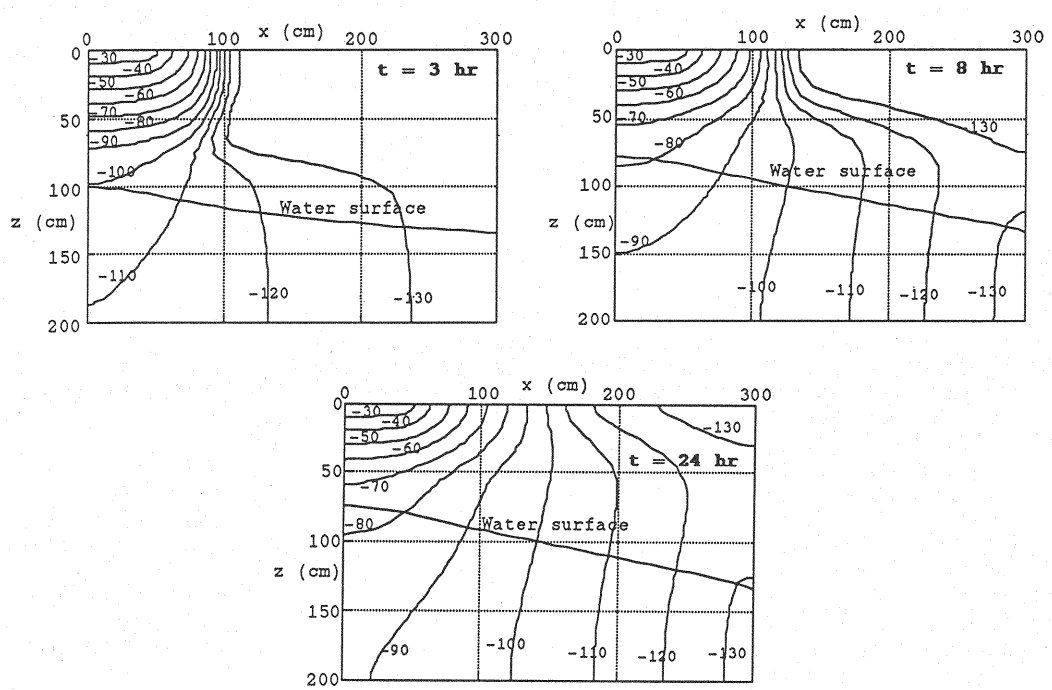

Fig. 18 Computed distribution of hydraulic head
at t = 3, 8, and 24 hr

mass balance error may not be as accurate as the present solution, in which the mass balance error is less than $1x10^{-5}$ (i.e. 0.001 %).

For reference purposes the calculated evolutions of moisture content at x = 5, 55, 105, and 155 cm are presented in Fig. 17. The distributions of the hydraulic head within the flow domain at times t = 3, 8, and 24 hr are shown in Fig. 18. Fig. 18 shows that the water keeps flowing upward to the right-hand-side upper corner of the domain. Such a flow continues as long as the hydraulic head at the lower part is greater than that at the upper one.

CONCLUSIONS

The following major conclusions can be drawn from the present study:

(a) The proposed model, which is developed for the mixed form of Richards' equation, ensures mass balance in its solution regardless of time step size and nodal spacings, and has no limitations when applied to field problems. Such a mass-conservative solution is, undoubtedly, more accurate than the corresponding ψ-based solution associated with mass loss.

(b) The Newton-Raphson iteration, when applied to the mixed form of Richards' equation, provides a convergence rate of second order. Owing to such a highly accurate linearization scheme, the proposed algorithms for nonlinear updating nodal pressure heads and for estimating initial nodal pressure heads are simple and efficient. Neither pressure head-based models, regardless of the iteration, nor mixed-based models using the modified Picard iteration provides a second-order accurate linearization. Therefore, these models can not be computationally as efficient as the present model.

(c) The proposed model is capable of incorporating boundary conditions of all types, including complex conditions along potential seepage faces, in a mass-conservative form.

REFERENCES

1. Allen, M.B. and C.L. Murphy : A finite-element collocation method for variably saturated flow in two space dimensions, Water Resources Research, Vol.22, No.11, pp.1537-1542, 1986.
2. Celia, M.A., E.F. Bouloutas and R.L. Zarba : A general mass-conservative numerical solution for the unsaturated flow equation, Water Resources Research, Vol.26, No.7, pp.1483-1496, 1990.
3. Cooley, R.L. : Some new procedures for numerical solution of variably saturated flow problems, Water Resources Research, Vol.19, No.5, pp.1271-1285, 1983.
4. Haverkamp, R., and M. Vauclin : A note on estimating finite difference hydraulic conductivity values for transient unsaturated flow problems, Water Resources Research, Vol.15, No.1, pp.181-187, 1979.
5. Haverkamp, R., M. Vauclin, J. Touma, P.J. Wierenga and G. Vachaud : A comparison of numerical simulation models for one-dimensional infiltration, Soil Science Society of America Journal, Vol.41, 285-294, 1977.
6. Hills, R.G., I. Porro, D.B. Hudson and P.J. Wierenga : Modeling one-dimensional infiltration into very dry soils, 1, Model development and evaluation, Water Resources Research, Vol.25, No.6, pp.1259-1269, 1989.
7. Hong, L.D., J. Akiyama, and M. Ura : Efficient and accurate numerical scheme for one-dimensional infiltration, Proceeding of the 36th Japanese Conference on Hydraulics, pp.441-446, 1992.
8. Huyakorn, P.S., E.P. Springer, V. Guvanasen and T.D. Wadsworth : A three-dimensional finite element model for simulating water flow in variably saturated porous media, Water Resources Research, Vol.22, No.13, pp.1790-1808, 1986.
9. Huyakorn, P.S., S.D. Thomas and B.M. Thompson : Techniques for making finite elements competitive in modeling flow in variably saturated porous media, Water Resources Research, Vol.20, No.8, pp.1099-1115, 1984.
10. Kaluarachchi, J.J. and J.C. Parker : An efficient finite element method for

modelling multiphase flow, Water Resources Research, Vol.25, No.1, pp.43-54, 1989.
11. McCord, J.T. : Application of second-type boundaries in unsaturated flow modeling, Water Resources Research, Vol.27, No.12, pp.3257-3260, 1991.
12. Narasimhan, T.N. and P.A. Witherspoon : Numerical model for saturated-unsaturated flow in deformable porous media, 3. Applications, Water Resources Research, Vol.14, No.6, pp.1017-1034, 1978.
13. Paniconi, C., A.A. Aldama and E.F. Wood : Numerical evaluation of iterative and non-iterative methods for the solution of the nonlinear Richards equation, Water Resources Research, Vol.27, No.6, pp.1147-1163, 1991.
14. Philip, J.R. : Theory of infiltration, Advanced Hydroscience, Vol.5, pp.216-291, 1969.
15. Rubin, J. : Theoretical analysis of two-dimensional, transient flow of water in unsaturated and partly unsaturated soils, Soil Science Society of America Journal, Vol.32, No.5, pp.607-615, 1968.
16. Vauclin, M., D. Khanji and G. Vachaud : Experimental and numerical study of a transient, two-dimensional unsaturated-saturated water table recharge problem, Water Resources Research, Vol.15, No.5, pp.1089-1101, 1979.

APPENDIX - NOTATION

The following symbols are used in this paper:

A = matrix of coefficients;

$C=d\theta/d\psi$ = specific moisture capacity;

$D=dK/d\psi$ = tangent slope of the K-ψ curve;

e_k = unit vector in the x_2 (or z) direction;

i, j = subscripts used to denote location of blocks;

I_n = number of iterations for the time level n

k = subscript used to denote tensor where k = 1, 2;

K = unsaturated hydraulic conductivity;

$K_{I,\ldots,IV}$ = hydraulic conductivities evaluated at the interblocks I, II, III, IV, respectively;

K_s = saturated hydraulic conductivity;

n = superscript used to denote time level;

n_k = outward unit vector normal to the boundary segment Γ_2;

N = number of blocks in the x_1 (or x) direction;

r = superscript used to denote iteration level;

R = residual vector;

t = time;

v_f = theoretical front velocity in Example 2;

V_k = Darcy velocity;

V_n = prescribed Darcy velocity normal to the boundary segment Γ_2;

V_{sf} = Darcy velocity normal to the potential seepage face;

$V_{I,\ldots,IV}$ = velocities normal to the interblocks I, II, III, IV, respectively;

x, z = Cartesian coordinates;

x_1, x_2 = Cartesian coordinates;

W_Γ = net cumulative flux into the flow domain through the boundary Γ;

W_Ω = change in total amount of water within the flow domain Ω;
Γ = boundary of the flow domain;
Γ_1 = Dirichlet boundary segment;
Γ_2 = Neumann boundary segment;
$\delta\psi$ = iterative increment in pressure head;
$\delta\boldsymbol{\psi}$ = unknown vector;
Δt = time step size;
Δt_{max} = maximum allowable time step size;
Δt_n = time step size for the time level n;
Δt_0 = initial time step size;
Δx, Δz = nodal spacings in the x, z direction, respectively;
ε = water content convergence tolerance;
ε_p = pressure head convergence tolerance;
ξ = coefficient in Eq. (24b);
η = empirical function used for updating of nodal pressure heads;
θ = volumetric moisture content;
ψ = pressure head;
ψ_0 = initial pressure head;
ψ_b = prescribed pressure head on the boundary segment Γ_1;
ψ_{sf} = pressure head on the potential seepage face;
$\chi = 0.6$ = empirical coefficient in the function η;
ω = time-weighting factor;
Ω = flow domain; and
* = superscript used to denote time-averaging.

(Received December 24, 1992; revised September 16, 1993)